Structures 34 (2021) 3851–3865

Contents lists available at ScienceDirect

Structures

journal homepage: www.elsevier.com/locate/structures

Structural properties of superior design solutions of steel buildings associated with BRBs

Jiro Takagi [a,*], Makoto Ohsaki [b], Yongsheng Cao [c]

[a] Graduate School of Urban Env. Sciences, Tokyo Metropolitan Univ., 1-1 Minami-osawa Hachioji, Tokyo 192-0397, Japan
[b] Graduate School of Engineering, Kyoto Univ., Kyoto 615-8540, Japan
[c] School of Civil Engineering, Guangzhou University, Guangzhou 510006, China

ARTICLE INFO

Keywords:
Steel buildings
Seismic design
Buckling restrained braces
Optimization
Energy dissipation

ABSTRACT

A design algorithm is proposed for rational seismic design solutions of steel buildings associated with buckling restrained braces (BRB). The strengths and locations of BRBs in addition to the section sizes of structural members are considered as discrete design variables. The steel volume including BRBs is minimized as an objective function under various practical design constraints. A seven-story office building is examined for application in two different types of structural systems, i.e. one mainly consisting of lateral frames and the other with limited utilization of lateral frames typically in perimeter separately from gravity frames. The derived solutions, defined as superior design solutions (SDSs), satisfy serviceability and limit-state constraints, taking into consideration the seismic energy dissipation effect of BRBs using the calculation of resistance and limit-state method. Their rationale is validated with response history analysis. Furthermore, the influences in SDSs by the seismic demand levels and elastic member constraint are investigated. The structural characteristics of SDSs associated with BRBs are objectively evaluated using the proposed design algorithm.

1. Introduction

Buckling restrained braces (BRBs) are widely used in regions of high seismic risk in the world. Using their seismic energy dissipation capacities, the acceleration responses in the buildings during large earthquakes are reduced and damage in the main frames can be restrained. Structural design procedures predicting responses of the buildings are developed with respect to the amount of damping effect during large earthquakes [1,2].

Seismic performance of coupled steel frame system (i.e. dual system) with moment resisting frames (MRFs) and BRBs have been studied since the early developing era of BRBs [3–5]. It was found that the dual system is effective against earthquakes, because the BRBs dissipate seismic energy and MRF reduces the residual displacement.

The research on BRBs has extended to various subjects such as effectiveness of BRBs for seismic reinforcement of existing RC frames [6–8] and probabilistic assessment [6,7] considering uncertainty of BRB properties. In these studies, analytical models of BRBs have been developed based on the experimental data. Also, there are studies on the design methodologies of steel buildings typically in dual systems with MRFs and BRBs. Freddi *et al.* [9] developed a single degree of freedom (SDOF) system for the parametric studies for BRB design to control residual displacements. Mehdipanah *et al.* [10] studied the rational lateral stiffness balance between the MRFs and BRBs. However, these studies do not focus on cost effectiveness in realistic buildings. Sarno and Elnashai [11] studied both seismic performance and cost, examining existing nine-story steel buildings comparing multiple design options; however, the design parameters are limited in brace types and locations.

In terms of existing research on using optimization for evaluation of the structures with BRBs, many of them focus on optimizing the strengths and/or locations of BRBs under the given main frame structures [12–15]. Fewer studies have been conducted for simultaneous optimization of BRBs and main frame. Rezazadeh and Talatahari [16] proposed multiobjective optimization method for minimizing the cost and damage under large earthquakes considering the yield strength of BRBs and section sizes of columns and beams as the discrete design variables. Abedini *et al.* [17] optimized the section sizes of columns and BRBs using heuristic methods called slap swarm algorithm and enhanced colliding bodies optimization. However, in these studies, only plane frame is considered, and seismic design constraints are limited in major issues such as inter-story drift ratios. Consequently, the obtained design solutions do not fully represent or applicable to the actual building design.

* Corresponding author.
E-mail addresses: jtakagi@tmu.ac.jp (J. Takagi), ohsaki@archi.kyoto-u.ac.jp (M. Ohsaki), 1111716007@e.gzhu.edu.cn (Y. Cao).

https://doi.org/10.1016/j.istruc.2021.10.006
Received 7 July 2021; Received in revised form 8 September 2021; Accepted 4 October 2021
Available online 13 October 2021

Nomenclature

List of Abbreviations

ASD	allowable stress design
BRB	buckling restrained brace
CBEB	calculation based on energy balance
CRLS	calculations of resistance and limit state
CULS	calculations of ultimate lateral strength
HSS	hollow structural section
MRF	moment resisting frame
MSLS	multiple-start-local-search
PFS	perimeter-frame system
RHA	response history analysis
RULS	required ultimate lateral strength
SBMF	steel braced moment frame
SDS	superior design solution
SDOF	single-degree-of-freedom
SFS	space-frame system
SMF	steel moment frame

List of Symbols

A_i	vertical lateral force distribution mode for the incremental lateral forces in pushover analysis
C_0	seismic base-shear coefficient for design seismic load
C_{max}	maximum story shear coefficient
C_{QU1}	base-shear coefficient at the ultimate lateral strength
C_{QUMF1}	base-shear coefficient at the ultimate lateral strength of the main frames without BRBs
F	design standard strength (nominal yield strength) of steel
F_h	reduction factor (=ratio between elastic and inelastic demand spectra) used in CRLS
D_f	coefficient representing structural ductility (ductility factor) used in CRLS
D_s	reduction factor of RULS
G_s	seismic amplification factor defined in CRLS
h	equivalent viscous damping factor
K_{1BRB}	initial axial stiffness of BRB
K_{2BRB}	post-yielding axial stiffness of BRB
K_a	ratio of elastic lateral stiffness provided by BRBs
K_f	stiffness of main frame
L	beam length
M_p	plastic moment
M_{pc}	plastic moment of column
M_{pb}	plastic moment of beam
N_{YBRB}	yielding axial force of BRB
Q_d	strength (capacity) of the equivalent SDOF system at serviceability limit used in CRLS
Q_s	strength (capacity) of the equivalent SDOF system at safety limit used in CRLS
R	inter-story drift ratio
R_{max}	maximum inter-story drift ratio
R_t	vibration characteristic factor
S_{abd}	acceleration response spectrum at bedrock defined in CRLS
S_{agf}	acceleration response spectrum at the ground surface defined in CRLS
T_1	first natural period
T_{MF1}	first natural period of the main frames without BRB
V_{BRB}	equivalent steel volume of BRB
V_{eq}	equivalent steel volume
Z	seismic zone factor
Z_p	plastic section modulus
δ	beam sagging displacement
$_{\Delta d}$	displacement of the equivalent SDOF system at serviceability limit used in CRLS
Δ_s	displacement of the equivalent SDOF system at safety limit used in CRLS
μ	ductility factor of the equivalent SDOF system ($=\Delta_s/\Delta_d$)
θ_R	maximum residual inter-story drift ratios

The authors obtained and evaluated the properties of optimal steel buildings using 3D analysis models taking into account many practical constraints including seismic design constraints against large earthquakes [18–20]. In these studies, design solutions are derived for different types of column shapes and lateral frame locations. Beam-to-column connections of steel buildings consist of two types: moment connections and pinned connections. The flanges of beams are rigidly connected to columns in the moment connections, while they are not connected in pinned connections. The lateral frames are composed of columns and beams with moment connections, and the gravity frames are composed of those with pinned connections. Most frames are the lateral frames in some countries like Japan, whereas lateral frames are limitedly placed typically in perimeter frames separately from gravity frames in other countries including the US. In this paper, the former system is referred to as the space-frame system (SFS) and the latter as the perimeter-frame system (PFS). Rectangular hollow structural section (HSS) columns are normally used in SFS, and I-shaped (wide flange) columns are used in PFS. Mele et al. [21] studied MRF steel buildings focusing on these frame systems i.e. perimeter and spatial; however, optimization method is not used for the compared steel design, and they used I-shaped column shapes which is different from Rectangular HSS studied in this paper for the spatial frame system. Past research [22,23] has focused on the differences of these systems; however, the buildings compared may not be equally and rationally designed and discussion on the findings of their structural characteristics may not always be objective.

In the practical process of seismic design, even finding a feasible solution satisfying all the constraints is difficult, because many structural and geometrical design requirements in serviceability and limit-state against large earthquakes are to be satisfied. The serviceability is checked with the allowable stress design (ASD), which is widely used for both new building design and existing building retrofit in Japan, based on the Japanese design standards. Also, the limit-state requirements are formulated under the design procedures of calculations of ultimate lateral strength (CULS) [19], and the calculations of resistance and limit state (CRLS) [20]. Because the design problem has many discrete design variables, a heuristic method rather than a mathematical programming approach is to be used. However, it is very difficult to handle many tight constraints in a heuristic method [24,25], although some methods have been proposed with relaxation of constraints [26]. To avoid convergence to an infeasible solution, the authors proposed a multiple-start-local-search (MSLS) algorithm to obtain approximate optimal solutions, which are called superior design solutions (SDSs), and applied it to find SDSs of SFS and PFS of seven-story office buildings. The steel volume is minimized and the design variables are the section sizes selected from a specified list of available sections [18–20]. The SDSs of SFS and PFS systems obtained through this algorithm are independent of designers' skills or experiences. Their structural characteristics are objectively discussed.

In this research, the Japanese structural design procedures including ASD, CRLS and CULS mainly for steel buildings are briefly overviewed for explanation of constraints in the MSLS algorithm. Then, the SDSs for the steel buildings associated with BRBs are derived for SFS and PFS using the MSLS algorithm in a similar manner as the authors' previous

work [20]. The CRLS is used for evaluation of the seismic performance against large earthquakes, taking into account the seismic energy dissipation capacities of BRBs. The section sizes of columns and beams in addition to the yield strengths and locations of BRBs are considered as the discrete design variables, and are simultaneously optimized. The characteristics of rational steel building design solutions associated with BRBs as well as the differences of SFS and PFS SDSs are objectively discussed, by comparing the top five solutions for both systems. Furthermore, the influence in the SDSs by the MSLS constraints, such as the seismic demand levels and the elastic main frame conditions is investigated.

2. Two-step seismic design procedure

The two-step seismic design procedure, which is commonly used for the seismic design practice in Japan and also used in this research, is overviewed in this section. The description below is not comprehensive but concise in order to provide the fundamental information for readers to understand the design procedure used in this research. Also, the explanation is limited to the design procedure for steel buildings with moderate sizes (not special buildings such as high-rise or seismically isolated building). More information about Japanese structural design procedure can be found in the monograph by Michel Bruneau et al. [27].

In Japan, the ASD procedure is commonly used for the seismic design against the small and moderate earthquakes (as well as design for the sustained load) [28]. Additionally, four seismic design procedures associated with inelastic analysis are prepared for the designs against large earthquakes, which are the CULS, CRLS, the calculation based on energy balance (CBEB), and response history analysis (RHA). For the design of buildings lower and smaller than certain height and floor area, the above-mentioned design procedure against larger earthquakes is not required and only ASD is performed. The two-step design procedure (ASD plus one of the four) is adopted for the design of larger or irregular buildings, e.g. steel buildings with more than 31 m of the height or irregular stiffness distribution. Among these four, CULS is the most common, while RHA is required for special buildings such as high-rise buildings and seismically isolated buildings.

In the design using ASD against the small or moderate earthquakes, the stresses in structural members under design seismic load are computed and it is confirmed that the stress values are smaller than the allowable stresses. The minimum and commonly adopted base shear coefficient of the ASD seismic design load is 0.2 or 0.3. Therefore, the design seismic lateral force is equivalent to 0.2 g or 0.3 g. In other words, buildings in Japan are elastically designed under 0.2 g or 0.3 g lateral design loads. The allowable stress in tension is 2/3 of the nominal strength of steel material for the design against sustained loads, and it is equal to the nominal strength for the design against combined seismic and sustained loads. The allowable stresses in compression and flexure are reduced with respect to the slenderness ratio considering flexural and lateral-torsional buckling. It is noteworthy that the live load (for the seismic design) is included in the calculations of the building weight for the seismic design loads. This is a difference from calculation in the equivalent lateral force procedure defined in ASCE7 [29].

The static pushover analysis is used in the CULS and CRLS design procedures. In CULS, it is confirmed that the computed ultimate lateral strength is greater than the required ultimate lateral strength (RULS), which is calculated using the reduction factor called D_s. The values of D_s are defined in Japanese design standards [30], and are varied with the structural systems. For instance, D_s values for steel moment frames (SMF) structures are 0.25–0.40 depending on the compositions of member ranks, which are defined with their width-to-thickness ratios, i.e. the plastic deformation capacity. This implies that RULSs are nearly equivalent to 0.25–0.40 g for regular steel moment frame buildings. The vertical and horizontal irregularities are taken into account and the penalty factors are multiplied to RULS for the irregular buildings. It may be noteworthy here that all moment frames designed in Japan correspond to "special moment frames" defined in ASCE7 [29].

The D_s values of steel braced moment frame (SBMF) buildings are 0.25–0.50, where Japanese SBMF is nearly equivalent to "dual systems with steel special moment frames and concentrically braced frames" defined in ASCE7. In addition to the ranks of beams and columns, two structural properties are taken into account for the D_s values for SBMF buildings, which are the compositions of brace ranks defined with their slenderness ratios and proportions of the seismic lateral forces carried by the braces.

The D_s factor is regarded as the reduction factor of RULS considering the plastic deformation capacity of the structure. The concept of D_s factor is similar to the reciprocal of R factor in ASCE7 [29], but is different in use. The D_s factor is used for the calculation of RULS, rather than the actual ultimate lateral strength calculated in the inelastic pushover analyses. Most beam-to-column connections are moment connections in Japanese steel buildings, and D_s values are defined only for SMF and SBMF for steel buildings. There is no other detailed categorization for steel buildings.

On the other hand, CRLS is a structural design procedure based on the Capacity Spectrum Method [31], more directly evaluating the energy dissipation effect of structures. Multi-story building structures are converted into equivalent single-degree-of-freedom (SDOF) systems using static pushover calculations. The lateral force restoring characteristics of the structures are represented by the acceleration-displacement response spectrum (the capacity spectrum). The response spectrum for the assumed earthquake (the demand spectrum) is reduced by considering the seismic energy dissipation effect, caused by member yielding and dampers such as BRBs as shown in Fig. 1. Therefore, CRLS is more suitable than CULS for the seismic design of buildings using BRBs. In CRLS, it is confirmed that the capacity is greater than the demand at the assumed limit-state, which is generally defined in terms of the maximum inter-story drift ratio, e.g., 1.5% or 2.0%, so that brittle failure does not occur under the inter-story drift ratio corresponding to the assumed limit-state. The outline of CRLS design procedure is explained by Kuramoto [32], and applications are demonstrated in reference [33].

3. Superior design solutions

SDSs of steel buildings are obtained by the MSLS method [34]. The design variables are the discrete yield strengths and locations of BRBs in addition to the discrete section sizes of beams and columns. The objective function to be minimized is the total steel volume of the building including the equivalent steel volume of BRBs described below. Constraints are given for the responses under the sustained load and those corresponding to two-step seismic design conditions. The MSLS procedure is illustrated in Fig. 2. Feasible solutions, which satisfy all constraints, are first obtained from approximately 10^7 random combinations of design variables. Note that most of the randomly generated solutions are rejected without carrying out structural analysis. In the next step, the ten best (minimum steel volume) feasible solutions are assigned as initial solutions for MSLS. The SDSs are defined as the top

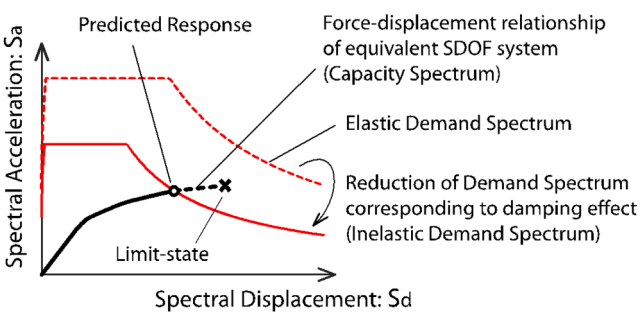

Fig. 1. Illustration of CRLS design procedure.

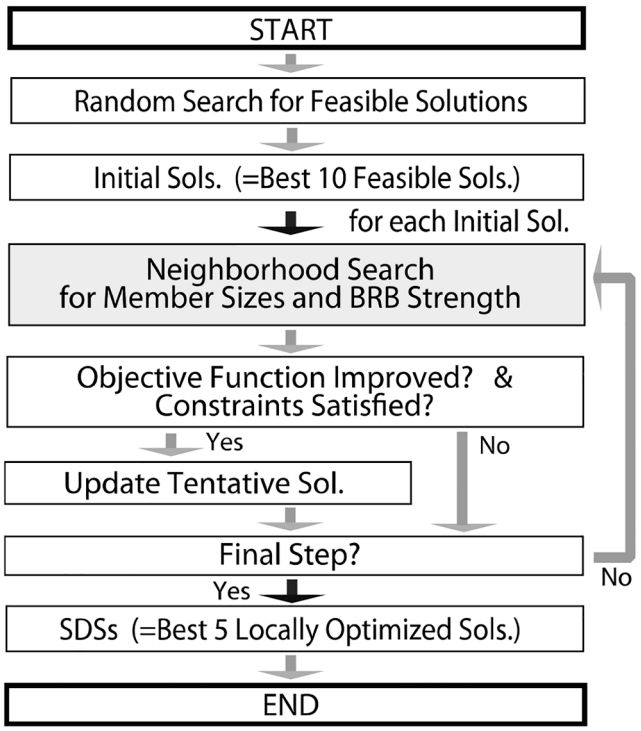

Fig. 2. MSLS algorithm.

five local optimal solutions obtained from the ten different initial solutions. The best solution is named as the 1st SDS that is primarily studied for its structural properties, and variations of properties are also evaluated comparing the five SDSs in the two structural systems, i.e., SFS and PFS. There are approximately 40 variables for members in main frames and BRBs, and approximately 100 geometrical and mechanical constraints. Because the ratio of number of combinations satisfying all constraints to the total number of combinations has a very small value between 10^{-5} and 10^{-4}, population based heuristic approaches such as the genetic algorithms are not effective for solving this problem.

A step-by-step update of design variables is assumed in MSLS. At each step of searching the solutions from a randomly generated initial solution, neighborhood solutions are generated by randomly increasing or decreasing the discrete variables of section sizes by one or stay the same within the range of each variable. Here, the number of neighborhood solutions is set as the same as the number of variables. The tentative solution is replaced with the best neighborhood solution, if it satisfies all constraints and improves the objective function value. When no better solution is found in the neighborhood, the tentative solution is carried over to the next step. The number of steps is 10,000. Therefore, the total number of neighborhood solutions is approximately 10,000 × 40 = 0.4 million. The constraints such as the width-to-thickness ratio are checked first without analysis and structural analysis is carried out for approximately 1/5 of the neighborhood solutions.

The superior solutions are not globally optimal. However, they are rationally obtained by the specified design algorithm, and therefore, independent of engineers' experience and preference. This research aims at identifying structural characteristics of steel frames associated with BRBs with different building structures and structural systems, in terms of the stiffness and strength balance between the main frames and BRBs as well as the locations of BRBs, by comparing the properties of superior solutions. Therefore, obtaining the strictly global optimal solution is not the primary interest of this research.

4. Application of MSLS

4.1. Outline of building examined

As shown in Fig. 3, a rectangular seven-story steel office building with 32.0 m × 19.2 m plan is examined. The building is simplified in order to identify general structural characteristics, and is the same as that examined in the authors' previous work [18–20]. The solid triangles in Fig. 3 indicate moment connections and the others represent pinned connections. All beam-to-column connections are moment connections and all frames are lateral frames in SFS, while four frames in the perimeters are the lateral frames and the others are the gravity frames in PFS. Fig. 4 shows the frame elevations with BRBs. The solid triangles in the columns on 2nd- and 5th-stories in Fig. 4 indicate the splices. The segments between the column splices are called "parts" and the member sections are grouped in each part. The names of columns and beams are

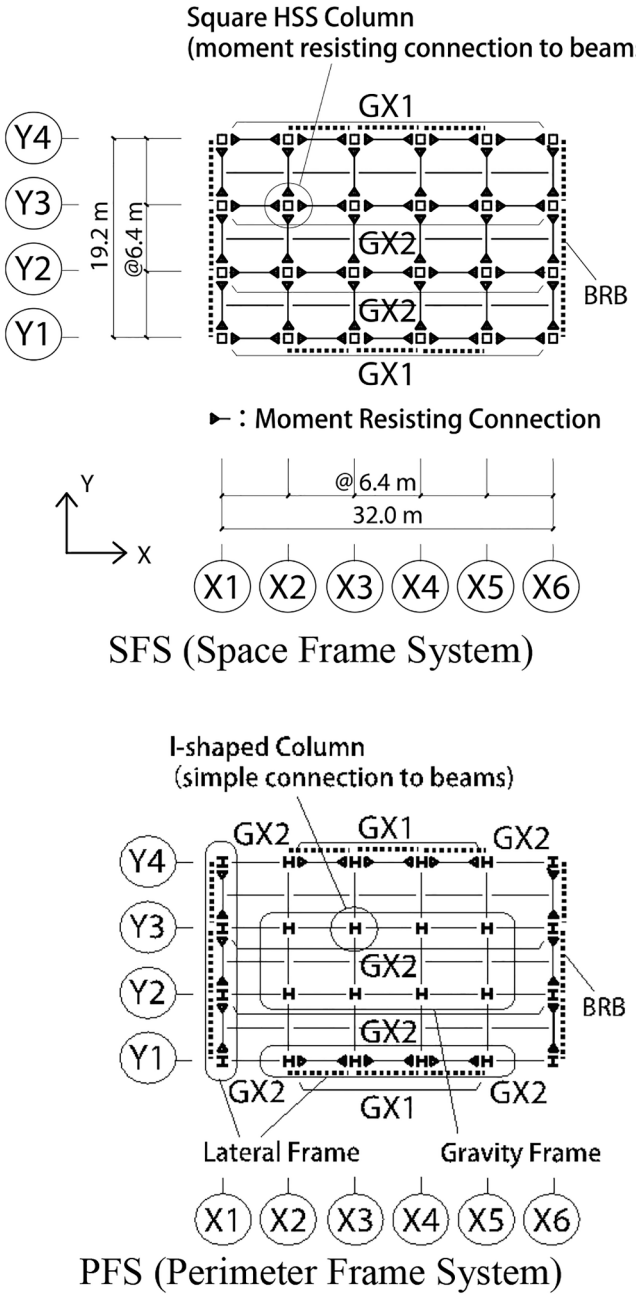

Fig. 3. Floor framing plan.

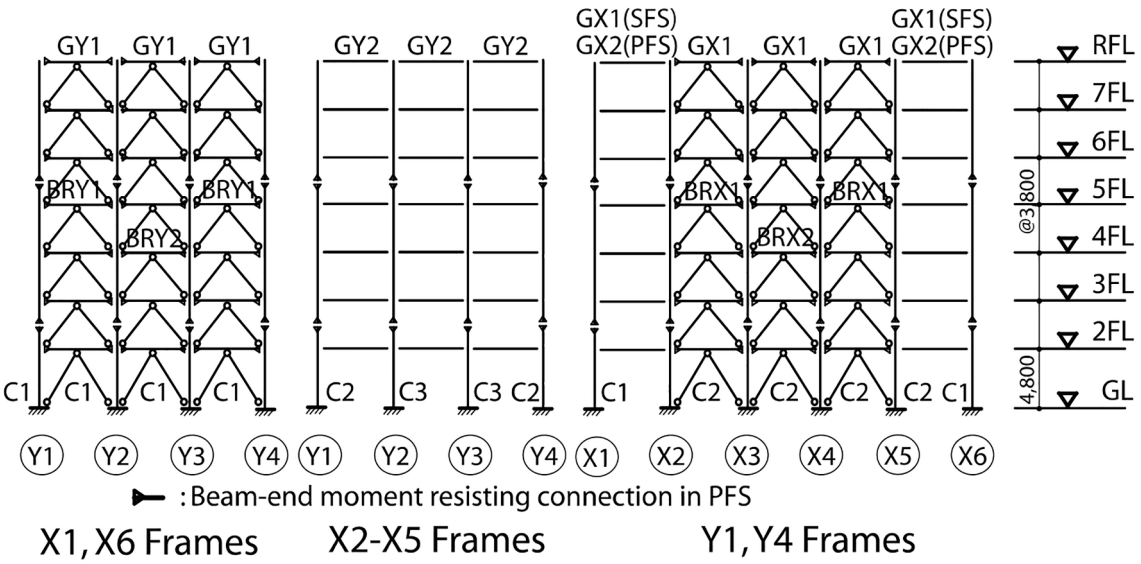

Fig. 4. Framing elevations.

shown in Figs. 3 and 4. GX2 and GY2 in the figures for PFS are pinned at the ends and designed only for the sustained load. However, these names are kept identical for comparison between the PFS and SFS.

Composite steel deck slabs are used for the floor structure in the building examined. The slabs are extended 400 mm from the perimeter axes shown in Fig. 3; therefore, the floor area is 656 m^2. The floor weights per unit area including the live load are 7.8 kN/m^2 and 6.8 kN/m^2 for the frame design and seismic design, respectively. The average exterior weight per unit elevation area is assumed as 2.0 kN/m^2. Therefore, the total weights per floor area are 9.0 kN/m^2 and 8.0 kN/m^2 for the frame design and seismic design, respectively. The weights are applied to the 3D frame models as concentrated loads at the nodes connecting beams and columns, and nodes at every 3.2 m in the beams. The roof weight is typically heavier than office floors but assumed to be the same for simplicity.

The grouped member sections are shown in Table 1. The columns are rectangular HSS in SFS and I-shaped sections in PFS. The beams are I-shaped sections for both SFS and PFS, and the braces are all BRBs. The steel grade of beams and columns is SN490, and the design standard strength, i.e., nominal strength, is 325 N/mm^2. Fig. 4 shows the possible locations of BRBs, which are the three spans in the four perimeter frames, i.e., all lateral frames in PFS. In the superior solutions, effective locations of BRBs are selected from the possible locations.

The possible ranges of discrete variables of section sizes and yield strength of BRBs are shown in Table 2. The section sizes are selected from the list of Japanese standard rolled sections [35] and built-up sections with steel plates with standard thickness. The discrete width and height of the sections in the columns and beams are assigned every 50 mm. The combinations of the flange width and thickness are defined as shown in the lower table in Table 2, where the cross-sectional area of flange A_f is considered as an independent variable.

Table 1
Member grouping in stories.

Part	Columns	Beams	BRBs
3	Mid. 5th Story – 7th Story	6th Floor - Roof	5th Story – 7th Story
2	Mid. 2nd Story – Mid. 5th Story	3rd Floor – 5th Floor	2nd Story – 4th Story
1	1st Story – Mid. 2nd Story	2nd Floor	1st Story

4.2. Modeling of frames

3D frame models are created for the elastic analysis for the ASD procedure and the inelastic pushover analysis for the CRLS. An in-house code is used for the elastic analysis and inelastic pushover analysis for obtaining SDSs using the MSLS. The accuracy has been verified in comparison to the results by a commercial analysis software Midas iGen [36].

Significance of this research lies in obtaining rational structural design applicable to actual building construction. Although the rational BRB locations in the SDSs could be found using 2D frame models, the structural characteristics are more directly evaluated with 3D SDSs incorporating the whole building compositions. This aspect is important in this research, because the main frame and BRBs are simultaneously designed in SDSs.

Modeling assumptions for the elastic analysis are summarized below.

(1) Floor diaphragm condition is adopted. The seismic lateral loads are given at the center of gravity in each floor.
(2) Columns are divided into two elements at the center of floors. Beams are divided every 3.2 m. The floor masses and gravity load are distributed in these beam nodes.
(3) The bottoms of 1st story columns are supported and rotationally fixed. The braces are pin connected.
(4) The composite effect between steel beams and concrete slabs is neglected.
(5) The fillet part of I-shaped sections is neglected.
(6) The rigid zone in the beam-to-column connections is neglected. Assuming reinforcing plates are properly welded at the panel zones in I-shaped columns, deformation in the panel zones is not considered.

The vertical distribution factor A_i defined in Eq. (1) [30] is adopted. The vibration characteristic factor R_t, and seismic zone factor Z [30] are both assumed to be 1.0. The seismic base-shear coefficient C_0 is 0.2 for the ASD.

$$A_i = 1 + \left(\frac{1}{\sqrt{\alpha_i}} - \alpha_i\right)\frac{2T}{1+3T} \tag{1}$$

where, α_i is the ratio of the building weight in ith and higher stories to the total building weight above the ground, and T is the first natural period that can be calculated as the building height (m) by the factor of

Table 2
Discrete MSLS variables.

Symbols	Members	Parts	Discrete variable options
D_c	Rectangular HSS columns	Width	Every 50 mm in 250–800 mm
t_c		Thickness	*1 (excluding 9 mm)
H_{wc}	I-shaped columns	Height	Every 50 mm in 300–900 mm
W_{fc}		Flange width	Every 50 mm in 300–700 mm
t_{wc}		Web thickness	*1
t_{fc}		Flange thickness	*1 (excluding 9 mm and 12 mm)
H_w	Beams	Height	Every 50 mm in 300–1000 mm
W_f		Flange width	Every 50 mm in 200–400 mm, *2
t_w		Web thickness	*1
t_f		Flange thickness	*1, *2
N_{YBRB}	BRB	Yield axial force	Every 500 kN in 0–3500 kN

	1	2	3	4	5	6	7	8	9	10	11	12
W_f (mm^2)	150	150	200	200	250	250	250	300	300	300	350	350
t_f (mm^2)	12	16	16	19	19	22	25	25	28	32	32	36
A_f (10^3mm^2)	1.8	2.4	3.2	3.8	4.8	5.5	6.3	7.5	8.4	9.6	11.1	12.6

*1: Plate thickness options are 9, 12, 16, 19, 22, 25, 28, 32, 36 and 40 mm.
*2: Combinational options of the flange width and thickness in beams are shown below.

0.03.

In addition to the above-mentioned modeling assumptions for elastic analyses, following assumptions are adopted for inelastic analysis

(1) Simple-step pushover analyses are conducted with the increments of lateral loads. i.e. No iterative calculation is performed in each load step.
(2) The increment of base shear coefficient in one step of the push-over analyses is approximately 0.002.
(3) Lumped rotational inelastic springs are placed at the ends of beams and columns. The springs are bilinear with sufficiently stiff initial stiffness and the post-yielding stiffness with 1/100 of the elastic flexural stiffness of the beams and columns.
(4) The yielding moment of the lumped rotational springs is defined as the plastic moment $M_p = 1.1FZ_p$, where F is the design standard strength (nominal yield strength) of the steel and Z_p is the plastic section modulus.
(5) The P-Delta effect is not taken into account. The safety limit is defined as 1.5% of inter-story drift and, under such lateral deformation, it is confirmed that the influence by the P-Delta effect in the lateral strength of the obtained SDSs is less than 3%.

The columns are considered to buckle when the fiber stress under sum of axial force ratio and flexural moment ratio reaches 1.0, where the axial force ratio is a ratio of the compressive stress to 1.1 times allowable compressive stress for temporary loads, and the flexural moment ratio is a ratio of the fiber stress to 1.1 times allowable flexural stress for temporary loads.

The buckling strength of beams is defined as the average of the tensile yield strength and buckling strength around the weak axis, by assuming that the upper flange of the beam is constrained by the slab and the lower flange is not. The axial forces of the beams are calculated as half of the sum of shear forces of inverted-V shaped concentrated braces, which are supposed to be transferred by the axial force of the connecting beams. The buckling lengths are assumed as the member lengths between the connecting nodes.

4.3. Modeling of BRBs

The BRBs are modeled as truss elements with bi-linear force restoring characteristics in the 3D frame models. The initial and post-yielding axial stiffness and the yielding axial force are denoted as K_{1BRB}, K_{2BRB} and N_{YBRB}, respectively. K_{1BRB} and K_{2BRB} are the total axial stiffness of combined BRB and connecting elements to the beams and columns. K_{2BRB} is defined as 2% of K_{1BRB}, which is greater than the post yielding stiffness of lumped plastic hinges in the columns and beams. It is because the strain hardening effect is more significant in BRBs [2]. Also, it is assumed that K_{1BRB} is proportional to N_{YBRB} as

$$K_{1BRB} = \alpha N_{YBRB} \tag{2}$$

Under this assumption, the number of design variables for a single BRB is reduced to one.

The initial axial stiffness of the series of BRB and connecting elements is calculated for several BRB products [37,38]. The average value of the ratio of N_{YBRB} to K_{1BRB} is 0.19 (1/mm), i.e., $\alpha = 0.19$ (1/mm) in Eq. (2). The first story height in the building examined is 4.8 m, which is higher than 3.8 m of the standard story height as shown in Fig. 4. However, $\alpha = 0.19$ (1/mm) for all stories reasonably works, because the axial stiffness of BRB is relatively lower than that of the connecting elements, and the difference in the stiffness of connecting elements in the first and other stories do not significantly affect the total axial stiffness. The equivalent steel volume of BRBs, denoted as V_{BRB}, is defined as

$$\begin{aligned} V_{BRB} &= 0 && \text{for} N_{YBRB} = 0 \\ V_{BRB} &= b_1 N_{YBRB} + b_2 && \text{for} N_{YBRB} \neq 0 \end{aligned}$$

Note that V_{BRB} is included in the total steel volume of the building as the objective function, and represents steel volume of all components in BRBs such as yielding steel core, buckling restraining tube and connecting elements. Hereinafter BRB component of any type is called "BRB member". V_{BRB} is essentially a cost indicator of BRBs, and the coefficients b_1 and b_2 in Eq. (3) are defined in view of the cost balance of BRBs to the normal steel of the main frames. There is no written reference on the cost and Eq. (3) is defined through hearing to engineers and manufacturers.

Based on the cost estimate of BRB products and steel volume of the connected elements, b_1 and b_2 are assigned as 6.0×10^{-5} m^3/kN and 0.12 m^3, respectively. For example, when $N_{YBRB} = 1000$ kN or 2000 kN, V_{BRB} is 0.18 m^3 or 0.24 m^3, respectively. Multiplying the specific weight and cost per unit weight of steel in the main frames of buildings to these numbers gives the estimated cost of BRB members, which reasonably agrees with the BRB cost in practice in Japan. Recognizing that definition of V_{BRB} significantly influences the superior solutions, Eq. (5) is adopted as one reasonable assumption.

The design options of N_{YBRB} vary from zero to 5000 kN in every 500 kN. The effective locations of BRBs are selected including $N_{YBRB} = 0$ for nonexistence of BRB. Evaluating V_{BRB} using Eq. (3), V_{BRB} has a smaller value for fewer BRBs with higher N_{YBRB} than more BRBs with lower N_{YBRB}, as observed in the real designs. Also, in order to accelerate the process of finding effective BRB locations, the probability of $N_{YBRB} = 0$ is set as 50% for finding the initial solutions in MSLS.

4.4. MSLS constraints

The constraints of MSLS are summarized in Table 3. The symbols are defined in Table 2.

(*1) The allowable stress is defined in the "AIJ Design Standard for Steel Structures" [28]. Beams are assumed to be laterally supported.

(*2) The width-thickness ratios for members with A or B rank [30] shall be satisfied.

(*3) Optimized I-shaped sections often have relatively large height with thin flange thickness. In order to avoid the sections significantly different from standard section sizes, the constraint of $t_f/t_w \geqq 1.3$ is introduced for the beams. This constraint is not applicable for the columns, where the uniform height is assumed and built-up sections may be used.

(*4) The sum of the plastic moment of columns ΣM_{pc} shall be greater than 1.5 times the sum of the plastic moment of beams ΣM_{pb} in each story. This is required by the Japanese code for cold-form rectangular HSS columns but not for I-shaped columns; however, this is applied for all columns in this research.

(*5) The beam sagging displacement δ shall be smaller than 1/300 of the beam length L.

(*6) The predicted lateral strength at the safety limit shall be greater than the strength defined in the demand spectrum, based on CRLS.

(*7) The beam heights in a floor shall be uniform in SFS, as in Japanese practice, thus simplifying the beam-to-column connection details with straight splices between the beam flanges and diaphragm plates in columns.

Some constraints refer to the section properties such as width-to-thickness ratios and strong-column-weak-beam conditions which can be evaluated without elastic structural analysis, and others refer to the structural responses such as inter-story drift ratios and allowable stress ratios. GX2 and GY2 beams are supported in pins at their ends as shown in Figs. 3 and 4, and have the section H-400 × 200 × 8 × 13, which is the minimum I-shaped rolled section that can carry the sustained load, and the section size of GX2 and GY2 is excluded from the variables. Hereinafter, I-shaped section sizes are shown in order of their height, flange width, web-thickness and flange thickness in millimeter. For example, the height, flange width, web-thickness and flange thickness of H-400 × 200 × 8 × 13 are 400, 200, 8 and 13 mm, respectively. The square HSSs are shown in order of their depth (=width) and thickness.

4.5. Seismic Performance Requirements under CRLS

The lateral force–displacement relationships simulated in pushover calculations are used in CRLS for the evaluation of seismic performance against large earthquakes. In this research, CRLS is executed by referring to the procedures in Refs. [30,32,33]. Major assumptions for CRLS are summarized below:

Table 3
MSLS constraints.

No.	Lateral System	Constraints	
1	All	Allowable stress constraints, $\sigma \leqq \sigma_a$	(*1)
2		Width-thickness constraints for beams and columns with A or B rank e.g. $D_c/t_c \leqq 31.4$	(*2)
4		$t_f/t_w \geqq 1.3$ for beams	(*3)
5		Strong-column-weak-beam constraint, $\Sigma M_{pc} \geqq \Sigma 1.5 M_{pb}$	(*4)
6		Beam sagging constraint, $\delta < L/300$	(*5)
7		Constraint for inter-story drift ratio under seismic design load, $R \leqq 0.5\%$	
8		CRLS	(*6)
9	SFS	Uniform beam height in a floor	(*7)
10		Uniform column width	
11	PFS	Uniform column height (non-uniform flange width)	

(a) The acceleration response spectrum at bedrock S_{abd} with 5% damping factor as shown in Fig. 5 is adopted.
(b) Soil type II [30] (the most common soil condition in Japan) is assumed. Multiplying the seismic amplification factor G_s to S_{abd}, the acceleration response spectrum S_{agf} at the ground surface is obtained as shown in Fig. 5 [30].
(c) The safety limit is defined as the state when the maximum inter-story drift ratio reaches 1.5% or any of columns buckles under the incremental lateral force distribution factor A_i defined in Eq. (1).
(d) The serviceability limit is defined as the state when any of BRB, column or beam yields.
(e) The reduction factor F_h, which is the ratio between the elastic and inelastic demand spectra in Fig. 1, is derived from [30]

$$F_h = \frac{1.5}{1 + 10h} \tag{4}$$

$$h = 0.25\left(1 - 1/\sqrt{D_f}\right) + 0.05 \tag{5}$$

$$D_f = \frac{\Delta_s Q_d}{\Delta_d Q_s} \tag{6}$$

where, h is the equivalent viscous damping factor, and D_f is a coefficient representing structural ductility (ductility factor). Also, Δ_s and Q_s are the displacement and strength (capacity) of the equivalent SDOF system at the safety limit. Similarly, Δ_d and Q_d are the displacement and strength at the serviceability limit.

5. Properties of SDSs

5.1. MSLS results

The section sizes and BRB yield strength of five SDSs obtained by MSLS of the building in Fig. 3 are shown in Tables 4 and 5 for SFS and PFS, respectively. Five SDSs for each of SFS and PFS are listed in the Tables. There are three spans in the perimeter lateral frames with BRBs, and the section sizes are grouped in three parts, which are the vertical classification as shown in Fig. 4 and Table 1. The obtained section sizes are shown in each cell for a group, where the section sizes in the third to first parts are listed in the first to third rows, respectively, corresponding to the vertical locations. The numbers for BRBs indicate the yield axial force N_{YBRB} (kN), and '-' symbol indicates no BRB existing in the corresponding part. In addition to the obtained BRB locations in the lateral frames in X and Y directions indicated in Fig. 3, the values of equivalent steel volume V_{eq} are also shown in Tables 4 and 5.

3D inelastic frame models are created for these SDSs using a commercial simulation software Midas iGen [36]. First, the elastic analysis for the allowable stress check is conducted. The stress ratios of the SDS members are shown in Tables 4 and 5 with parentheses. Three load combinations considered here are the sustained load and the sustained load in addition to seismic loads for X and Y directions, respectively, which are indicated in Fig. 3. Hereinafter, the combined sustained load and seismic loads in X and Y direction, respectively, are simply called "X seismic load" and "Y seismic load". The seismic loads are defined for design against small and moderate earthquakes, and their base shear coefficient is 0.2, i.e., the lateral loads are equivalent to 0.2 g.

Seven different combinations of BRB locations are observed in total in the SDSs of SFS and PFS as shown in Tables 4 and 5. The locations in the 1st SDSs of SFS and PFS in both X and Y directions are identical, in which the BRBs are placed in the middle span in the 1st and 3rd parts, and are placed in the side spans in the 2nd part. This BRB location is obtained in eight lateral frames as shown in red in Tables 4 and 5 among 20 independent lateral frames in X and Y directions in SFS and PFS. Considering the member grouping, the obtained location is regarded as checkerboard pattern, avoiding vertically continuous placement of the BRBs. This BRB location is effective for resisting lateral forces reducing

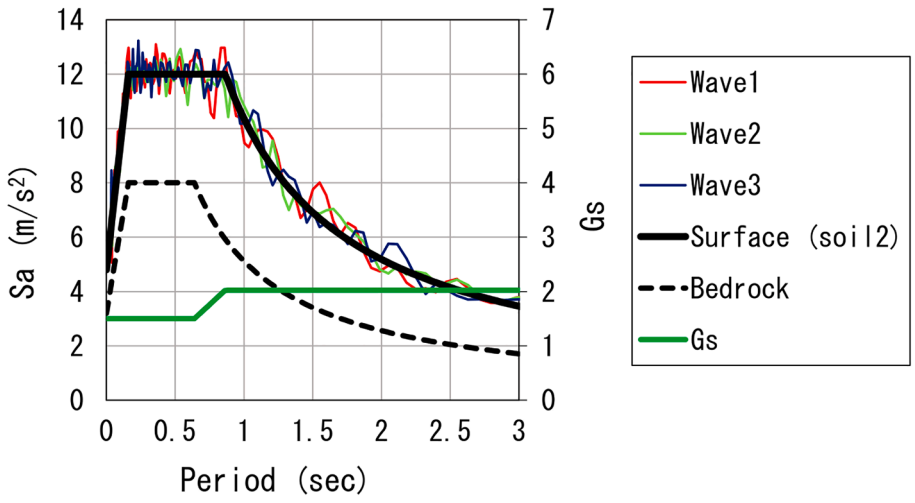

Fig. 5. Acceleration response spectra of ground motions under 5% damping constant.

additional axial forces in the columns.

No BRB exists in the first story in the lateral frames in X direction in 5th SDSs of both SFS and PFS. Consequently, the C2 columns and GX1 beams of PFS in the 2nd floor in these frames are significantly larger than those in other SDSs. The 5th SDSs satisfy CRLS and other MSLS constraints; however, the inter-story drifts and ductility factors in the first story in these frames are larger in RHA as shown later in Section 5.4. On the other hand, alternative SDSs shown in Section 5.7 may be more acceptable, where inelastic deformation in the main frames is refrained and seismic energy dissipation effect is more expected in BRBs.

5.2. Structural characteristics

The stress ratios, which are the ratios of the stresses under the three load combinations, respectively, to the allowable stress, are shown in Tables 4 and 5. "L", "X" and "Y" in the brackets indicate the dominating load combinations among sustained load, X seismic load and Y seismic load, respectively, which correspond to the highest stress ratios. It is noteworthy that the allowable stress for the sustained load is 2/3 of that for the seismic loads [28] and therefore the sustained load can be dominant, although X and Y seismic loads include the sustained load. The axial compression ratios of the columns, which are the ratios of compressive stress under the sustained load to the yield stress, are less than 0.49 for SFS and 0.37 for PFS. The stress ratios of BRBs are close to 1.0. Therefore, X and Y seismic loads control the BRB design.

Next, focusing on the 1st SDSs of SFS and PFS, inelastic pushover analysis results are discussed. The modeling assumptions are essentially the same as those for MSLS calculations; however, there is a difference in the iterations in the incremental load steps. In MSLS, no iteration is performed and the unbalanced loads are carried over to the next increment for reducing the computational cost, while the unbalanced loads are reduced by Newton iterations in inelastic analysis using Midas iGen. Thanks to the strong-column-weak-beam constraint, columns remain elastic at their safety limits of 1.5% inter-story drift ratio. Ductility factor for beam is defined as the ratio of element rotation angle at the safety limit to that at yielding, and the ductility factor for BRBs is the ratio of axial deformation at the safety limit to the yielding axial deformation. In the 1st SDSs, the ductility factors of beams and BRBs are less than 2.0 and 8.0, respectively. The maximum ductility factor of beams in SFS is 2.24, which is slightly greater than 1.68 in PFS. These values are smaller than the ultimate ductility factor for general beams, which is around 6 [33]. Also, the maximum ductility factors of BRBs for SFS and PFS are 7.57 and 7.69, respectively. With these values, it is confirmed that excessive ductile deformation is not required under the specified safety limit.

5.3. CRLS results

The relationships between the lateral forces and displacements of each story obtained from the pushover calculations of the 1st SDSs are converted to the representative relationship in an equivalent SDOF system [32,33], which is defined as "capacity spectrum" as shown in Fig. 1.

The calculated capacity spectra of SDSs are plotted in Fig. 6. The diamond at the end of capacity spectrum indicates the safety limit, and the square indicates the serviceability limit, which mostly corresponds to yielding of BRBs rather than yielding of columns and beams. The circle is the predicted response, which is obtained as the intersection of the capacity spectrum and the reduced demand spectrum with the reduction factor F_h defined in Eqs. (1)–(3). Fig. 6 shows that the safety limits (diamonds) and predicted responses (circles) are close in all cases. Therefore, it is seen that the obtained SDSs are highly controlled by CRLS.

Let C_{QU1} denote the base-shear coefficient at the ultimate lateral strength, which is defined as a lateral strength at the maximum inter-story drift reaching 1.25%. The values of C_{QU1} are 0.36 and 0.32 for X and Y dirs., respectively, in SFS, and 0.29 and 0.31 for X and Y dirs., respectively, in PFS. As seen from Fig. 6, PFS has smaller values of C_{QU1} and F_h than SFS. Therefore, more energy is dissipated by BRBs in SDS of PFS than SFS.

C_{QU1} of the main frames without BRBs C_{QUMF1} is calculated as 0.11 for both X and Y dirs. in SFS, and 0.034 and 0.060 for X and Y dirs. respectively in PFS. The base-shear coefficient of design seismic load C_0 is 0.2, and C_{QUMF1} is 55% of C_0 for SFS and 17–30% for PFS. The SEI/ASCE 7–16 [29] requires that the moment resisting frame (MRF) should be capable of resisting at least 25% of the prescribed seismic force in dual systems composed by BRBs and MRF. The quantitative evaluation between the design seismic load and prescribed seismic force in SEI/ASCE is difficult due to the difference of the design procedures; however, it is noteworthy that the SDSs of PFS may not satisfy the SEI/ASCE requirement.

Defining the ductility factor μ of the equivalent SDOF system as the ratio of the lateral displacement Δ_s at the safety limit to the displacement Δ_d at the serviceability limit, i.e., $\mu = \Delta_s/\Delta_d$, the values of μ for X and Y directions are 4.43 and 4.68 for SFS and 4.35 and 4.39 for PFS, which are within the allowable range. The equivalent natural periods at the safety limits are 1.44 and 1.55 for X and Y dirs., respectively, in SFS, and 1.62 and 1.50 for X and Y dirs., respectively, in PFS.

Table 4
Superior design solutions of space frame system (SFS).

	1	2	3	4	5
C1	350×350×12(0.55)[Y]	300×300×12(0.61)[L]	300×300×12(0.65)[L]	300×300×12(0.60)[L]	350×350×12(0.61)[Y]
	350×350×12(0.85)[Y]	300×300×12(0.90)[Y]	300×300×28(0.49)[Y]	300×300×12(0.89)[Y]	350×350×12(0.86)[Y]
	350×350×16(0.82)[Y]	300×300×19(0.96)[Y]	300×300×19(0.91)[Y]	300×300×28(0.75)[Y]	350×350×16(0.81)[Y]
C2	350×350×12(0.56)[X]	250×250×22(0.53)[L]	250×250×12(0.85)[X]	300×300×12(0.65)[L]	500×500×19(0.25)[X]
	350×350×12(0.82)[X]	250×250×19(0.90)[X]	250×250×19(0.92)[X]	300×300×19(0.76)[X]	500×500×22(0.37)[X]
	350×350×22(0.66)[X]	250×250×22(0.83)[X]	250×250×28(0.69)[X]	300×300×32(0.65)[X]	500×500×32(0.96)[X]
C3	300×300×22(0.22)[L]	300×300×12(0.37)[L]	300×300×12(0.38)[L]	250×250×12(0.49)[L]	250×250×12(0.48)[L]
	300×300×12(0.71)[L]	300×300×12(0.70)[L]	300×300×12(0.71)[L]	250×250×12(0.88)[L]	250×250×16(0.68)[L]
	300×300×12(0.86)[L]	300×300×16(0.66)[L]	300×300×12(0.85)[L]	250×250×19(0.72)[L]	250×250×25(0.76)[X]
GX1	300×250×9×19 (0.43)[X]	300×150×9×12 (0.72)[X]	300×150×9×12 (0.68)[L]	300×150×9×12 (0.88)[X]	300×150×9×12 (0.72)[L]
	300×200×9×16 (0.48)[X]	300×150×9×16 (0.56)[L]	350×200×12×16(0.47)[X]	300×250×9×19 (0.57)[X]	350×150×12×16(0.49)[X]
	400×250×12×19(0.34)[X]	350×150×12×16(0.45)[L]	300×250×9×19 (0.32)[L]	450×200×12×19(0.37)[X]	450×200×12×16(0.69)[X]
GX2	300×150×9×12 (0.93)[L]	300×150×9×12 (0.90)[L]	300×150×9×12 (0.96)[L]	300×150×9×16 (0.78)[L]	300×150×9×12 (0.90)[L]
	300×200×9×16 (0.58)[L]	300×200×9×16 (0.56)[L]	350×150×9×12 (0.81)[L]	300×150×9×12 (0.90)[L]	350×150×9×12 (0.71)[L]
	400×200×9×19 (0.35)[X]	350×250×9×19 (0.34)[L]	300×250×9×19 (0.40)[L]	450×150×9×12 (0.52)[L]	450×150×9×16 (0.59)[X]
GY1	300×150×9×12 (0.70)[Y]	300×150×9×16 (0.56)[L]	300×150×9×12 (0.69)[L]	300×200×9×19 (0.39)[L]	300×250×9×22 (0.41)[Y]
	300×150×9×16 (0.55)[L]	300×250×9×19 (0.39)[Y]	350×250×12×19(0.41)[Y]	300×250×9×22 (0.35)[Y]	350×250×12×19(0.27)[Y]
	400×200×12×16(0.31)[Y]	350×200×12×19(0.34)[Y]	300×250×9×25 (0.32)[Y]	450×250×12×19(0.32)[Y]	450×150×12×16(0.33)[Y]
GY2	300×150×9×12 (0.94)[L]	300×150×9×12 (0.91)[L]	300×150×9×12 (0.93)[L]	300×150×9×12 (0.95)[L]	300×150×9×12 (1.00)[L]
	300×150×9×12 (0.91)[L]	300×200×9×16 (0.56)[L]	350×150×9×16 (0.60)[L]	300×150×9×16 (0.76)[L]	350×150×9×12 (0.82)[L]
	400×200×9×16 (0.43)[Y]	350×200×9×16 (0.48)[L]	300×250×9×19 (0.41)[L]	450×150×9×16 (0.46)[Y]	450×150×9×16 (0.50)[Y]
BRX1	–	–	–	1000(0.84)[X]	–
	1500(0.86)[X]	1500(0.87)[X]	1500(0.88)[X]	1500(0.84)[X]	2000(0.87)[X]
	–	3000(0.56)[X]	2500(0.66)[X]	2000(0.78)[X]	–
BRX2	2000(0.78)[X]	2000(0.82)[X]	2000(0.80)[X]	–	1500(0.99)[X]
	–	–	–	–	–
	3500(0.85)[X]	–	–	–	–
BRY1	–	1000(0.96)[Y]	1000(0.97)[Y]	1000(0.95)[Y]	–
	1500(0.91)[Y]	–	–	–	1500(0.90)[Y]
	–	2000(0.83)[Y]	–	–	–
BRY2	2000(0.82)[Y]	–	–	–	1500(0.98)[Y]
	–	3000(0.82)[Y]	3000(0.82)[Y]	3000(0.83)[Y]	–
	3000(0.98)[Y]	–	3500(0.90)[Y]	3000(0.99)[Y]	3000(0.89)[Y]
V_{eq}	44.3 m^3	44.6 m^3	45.1 m^3	46.3 m^3	47.7 m^3
T_1	0.89 (X), 0.94 (Y)	0.89 (X), 0.96 (Y)	0.89 (X), 0.93 (Y)	0.99 (X), 0.95 (Y)	1.00 (X), 0.94 (Y)
T_{MF1}	2.69 (X), 3.21 (Y)	3.13 (X), 3.08 (Y)	3.02 (X), 2.92 (Y)	2.89 (X), 3.02 (Y)	2.55 (X), 2.61 (Y)
K_a/K_f	8.2 (X), 10.7 (Y)	11.5 (X), 9.4 (Y)	10.6 (X), 8.9 (Y)	7.5 (X), 9.2 (Y)	5.6 (X), 6.8 (Y)
X	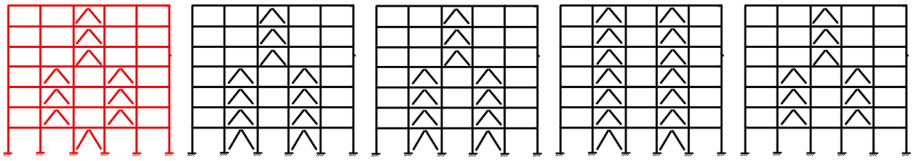				
Y	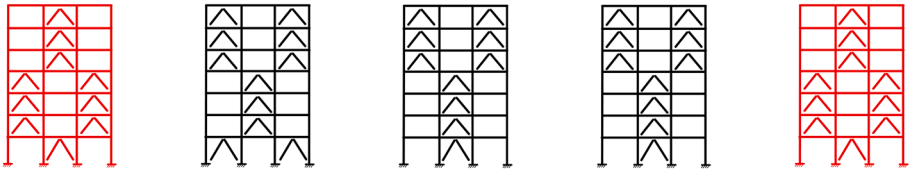				

5.4. Response history analysis

RHA is conducted for the SDSs to evaluate their structural characteristics using a commercial software SNAP [39]. The modeling assumptions are basically the same as those used in the static pushover analysis model. The damping factor is assigned as 2% for the first natural period, and the tangent stiffness proportional damping matrix is used.

Three ground motions for very rare earthquakes are generated to fit the response spectrum defined in Fig. 5. The phases of waves are randomly assigned and the duration is 50 s. The acceleration spectra of these ground motions are superimposed in Fig. 5. The time increment in RHA is 0.005 sec., and Newmark β method (β = 1/4) is used for the time integration.

Fig. 7 shows the mean values of maximum inter-story drift ratio R_{max} of five SDSs under the three seismic ground motions. The responses in X and Y directions are both plotted in one figure separately for SFS and PFS. R_{max} of 1st story in 5th SDS of SFS in X direction has a significantly large value that is close to 2% due to absence of the BRB in the 1st part. The averages of R_{max} in five SDSs in both X and Y directions are 1.52% for SFS and 1.54% for PFS. They are close to the predicted response which is equal to the inter-story drift ratio given for the limit-state in CRLS. Fig. 8 shows cumulative distribution of R_{max} for SFS and PFS, and normal distribution for reference. The distribution of SFS exhibits a slightly larger variation of responses than PFS.

Fig. 9 shows the mean values of maximum story shear coefficient C_{max} of five SDSs under the three seismic ground motions. The vertical lateral force distribution mode A_i, used in the pushover simulations, is superimposed with the base-shear coefficient equal to 0.3. It is confirmed that C_{max} values are greater than A_i in the higher stories.

Fig. 10 shows the mean values of maximum residual inter-story drift ratios θ_R of five SDSs under the three seismic ground motions. The mean values of θ_R in five SDSs in both X and Y directions are 0.24% for SFS and 0.30% for PFS, i.e., PFS has a larger θ_R value than SFS. However, these values are within tolerance and the residual deformation can be repaired after the large earthquakes.

The maximum ductility factors of structural elements including

Table 5
Superior design solutions of perimeter frame system (PFS).

	1	2	3	4	5
C1	400×300×12×16(0.68)[Y]	450×300×12×19(0.61)[Y]	400×300×12×25(0.49)[Y]	600×350×16×19(0.41)[Y]	450×400×12×28(0.20)[Y]
	400×400×12×22(0.63)[Y]	450×300×12×36(0.56)[Y]	400×300×12×32(0.63)[Y]	600×350×16×19(0.61)[Y]	450×350×12×19(0.63)[Y]
	400×400×12×32(0.68)[Y]	450×300×12×36(0.74)[Y]	400×300×12×36(0.70)[Y]	600×300×16×36(0.76)[Y]	450×400×12×36(0.73)[Y]
C2	350×300×12×19(0.63)[X]	350×300×12×16(0.71)[X]	550×300×16×16(0.56)[X]	450×300×12×22(0.51)[X]	600×300×16×16(0.53)[X]
	350×300×12×28(0.73)[X]	350×300×12×25(0.82)[X]	550×350×16×19(0.65)[X]	450×300×12×22(0.81)[X]	600×300×16×22(0.71)[X]
	350×350×12×28(0.88)[X]	350×350×12×28(0.89)[X]	550×300×16×36(0.85)[X]	450×350×12×28(0.92)[X]	600×600×16×32(0.94)[X]
C3	350×300×12×25(0.29)[L]	300×300×9×16 (0.45)[L]	350×300×12×19(0.36)[L]	300×300×9×16 (0.45)[L]	400×300×12×19(0.35)[L]
	350×300×12×19(0.72)[L]	300×300×9×22 (0.69)[L]	350×300×12×16(0.82)[L]	300×300×9×22 (0.69)[L]	400×300×12×19(0.70)[L]
	350×300×12×22(0.84)[L]	300×300×9×22 (0.89)[L]	350×300×12×32(0.61)[L]	300×300×9×28 (0.72)[L]	400×300×12×22(0.84)[X]
GX1	300×150×9×12 (0.70)[X]	300×150×9×16 (0.64)[X]	300×200×9×16 (0.55)[X]	350×150×12×16(0.61)[X]	400×200×12×16(0.51)[X]
	300×150×9×16 (0.54)[L]	300×250×9×22 (0.28)[X]	300×200×9×16 (0.41)[L]	350×200×12×16(0.37)[X]	300×200×9×16 (0.41)[L]
	350×250×12×22(0.26)[X]	400×250×12×22(0.25)[X]	350×250×12×25(0.28)[X]	400×250×12×22(0.29)[X]	650×250×19×25(0.53)[X]
GX2	400×200×8×13 (0.90)[L]	400×200×8×13 (0.90)[L]	400×200×8×13 (0.90)[L]	400×200×8×13 (0.90)[L]	400×200×8×13 (0.90)[L]
	400×200×8×13 (0.90)[L]	400×200×8×13 (0.90)[L]	400×200×8×13 (0.90)[L]	400×200×8×13 (0.90)[L]	400×200×8×13 (0.90)[L]
	400×200×8×13 (0.90)[L]	400×200×8×13 (0.90)[L]	400×200×8×13 (0.90)[L]	400×200×8×13 (0.90)[L]	400×200×8×13 (0.90)[L]
GY1	300×200×9×16 (0.55)[Y]	300×150×9×12 (0.70)[Y]	300×150×9×16 (0.63)[Y]	400×200×12×16(0.53)[Y]	300×150×9×12 (0.65)[L]
	350×200×12×19(0.34)[Y]	300×200×9×19 (0.37)[Y]	300×150×9×16 (0.53)[L]	350×200×12×16(0.39)[Y]	400×200×12×19(0.45)[Y]
	600×250×16×22(0.24)[Y]	300×150×9×12 (0.26)[Y]	300×200×9×16 (0.41)[L]	350×250×12×19(0.34)[Y]	450×250×12×25(0.37)[Y]
GY2	400×200×8×13 (0.90)[L]	400×200×8×13 (0.90)[L]	400×200×8×13 (0.90)[L]	400×200×8×13 (0.90)[L]	400×200×8×13 (0.90)[L]
	400×200×8×13 (0.90)[L]	400×200×8×13 (0.90)[L]	400×200×8×13 (0.90)[L]	400×200×8×13 (0.90)[L]	400×200×8×13 (0.90)[L]
	400×200×8×13 (0.90)[L]	400×200×8×13 (0.90)[L]	400×200×8×13 (0.90)[L]	400×200×8×13 (0.90)[L]	400×200×8×13 (0.90)[L]
BRX1	–	–	–	–	–
	1500(0.93)[X]	1500(0.92)[X]	1500(0.92)[X]	1500(0.93)[X]	2000(0.84)[X]
	–	–	–	–	–
BRX2	2000(0.87)[X]	2000(0.86)[X]	2000(0.84)[X]	2000(0.85)[X]	2000(0.80)[X]
	–	–	–	–	–
	3500(0.88)[X]	3500(0.89)[X]	3500(0.83)[X]	3000(0.99)[X]	–
BRY1	–	–	–	–	1000(0.98)[Y]
	1500(0.91)[Y]	1500(0.94)[Y]	1500(0.93)[Y]	1500(0.93)[Y]	–
	–	1000(0.77)[Y]	3000(0.57)[Y]	2000(0.78)[Y]	–
BRY2	2000(0.86)[Y]	2000(0.87)[Y]	2000(0.88)[Y]	2000(0.83)[Y]	–
	–	–	–	–	3000(0.85)[Y]
	3500(0.86)[Y]	2500(0.72)[Y]	–	–	3000(0.92)[Y]
V_{eq}	45.8 m^3	46.4 m^3	47.2 m^3	47.2 m^3	48.3 m^3
T_1	0.93 (X), 0.91 (Y)	0.94 (X), 0.90 (Y)	0.91 (X), 0.89 (Y)	0.94 (X), 0.89 (Y)	0.94 (X), 0.93 (Y)
T_{MF1}	4.72 (X), 3.53 (Y)	4.03 (X), 4.45 (Y)	3.87 (X), 4.82 (Y)	3.69 (X), 3.37 (Y)	3.12 (X), 3.37 (Y)
K_a/K_f	24.4 (X), 14.1 (Y)	17.4 (X), 23.7 (Y)	17.2 (X), 28.5 (Y)	14.4 (X), 13.4 (Y)	9.9 (X), 12.2 (Y)
X	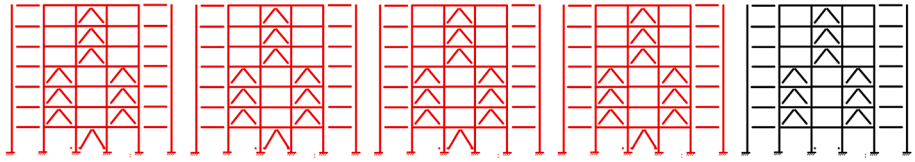				
Y	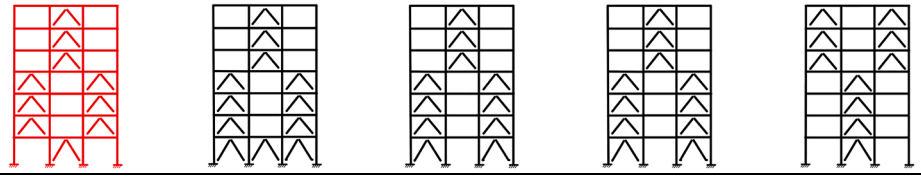				

columns, beams and BRBs, computed as the mean values of maximum ductility factors in three ground motions, are shown in Table 6. Because there is no BRB in the 1st part (=1st story) of lateral frames in X direction of both SFS and PFS, the ductility factors of the columns in the part are as high as 2.53 for SFS and 2.12 for PFS. The columns yield in limited cases only at the 1st story with the ductility factors less than 1.3 in both SFS and PFS. The ductility factors of beams are lower than 4, which is the upper bound in a common beam design criterion in Japanese practice. The ductility factors of BRBs are between 5.9 and 8.0 in SFS, while they are distributed in larger values between 6.7 and 8.7 in PFS.

5.5. Steel volume

Composition of the total steel volume V_{eq} of SDSs in Tables 4 and 5 is shown in Fig. 11. The volume of BRBs is computed using the equivalent value V_{eq} in Eq. (5) is shown as "1.0-SDS" in Fig. 11, where "1.25-SDS", "1.5-SDS" and "EF-SDS" are also shown and explained below. The values of V_{eq} of the 1st SDSs are 44.2 m^3 for SFS, while that of PFS is 45.8 m^3 which is 4% larger than SFS. Although the uniform beam height constraints are assigned in SFS, it does not cause any increase of steel volume under the uniform column spacing in both X and Y directions. The equivalent steel volume of BRBs is higher in PFS, because more lateral force is carried by the main frames in SFS. The difference of V_{eq} between the 1st and 5th SDSs is relatively small as 7.8% in SFS and 5.4% in PFS. Therefore, the BRB locations do not necessarily govern the overall steel volume.

Assuming that the section sizes of secondary beams, which are supported by the primary beams but not columns, are all H-350×175×7×11, the total steel volume of secondary beams in the building is 5.51 m^3. The steel volumes of through-diaphragm plates in SFS and continuity plates in PFS in the column-to-beam connections are roughly calculated as 2.5 m^3 and 1.2 m^3, respectively [18]. In addition, including assumed 30% extra miscellaneous steel, the total steel volume is 67.9 m^3 and 68.3 m^3 for SFS and PFS, respectively. The corresponding steel weight per unit area of floor is 116 kg/m^2 and 117 kg/m^2. Statistics [40] shows that the average steel weight in Japanese steel office

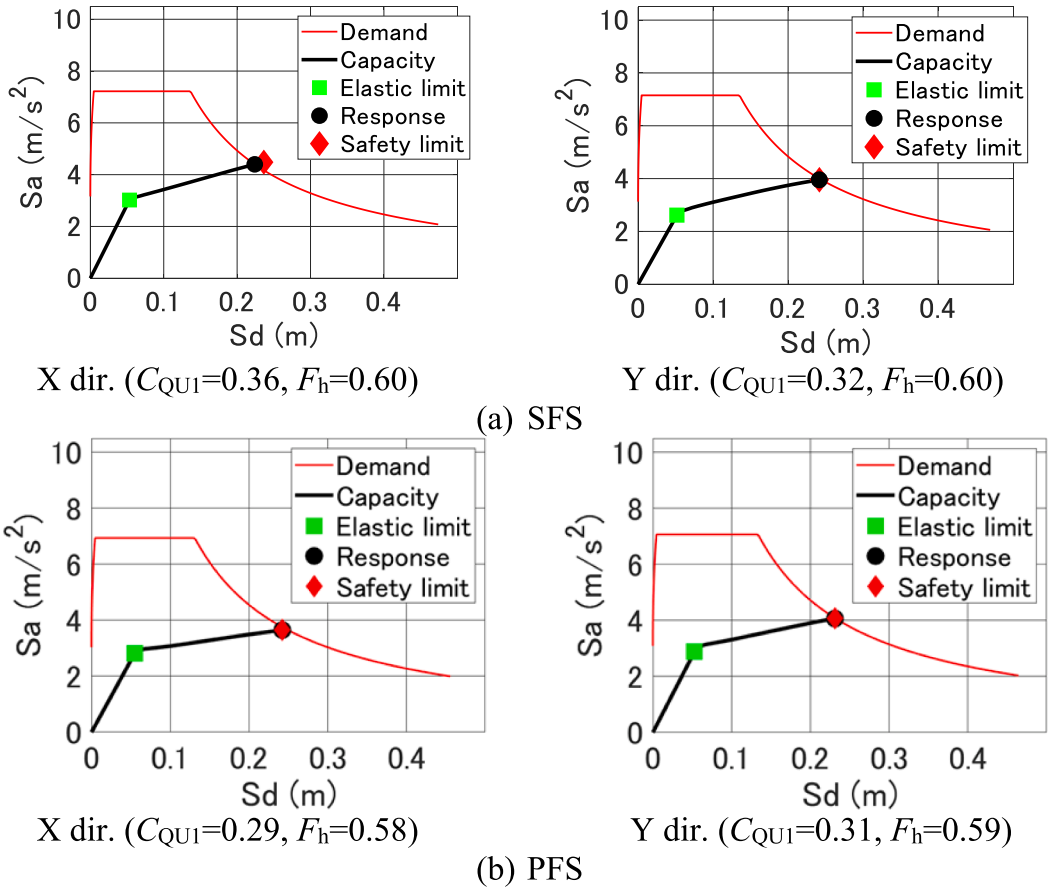

Fig. 6. S_a-S_d relationships of SDSs.

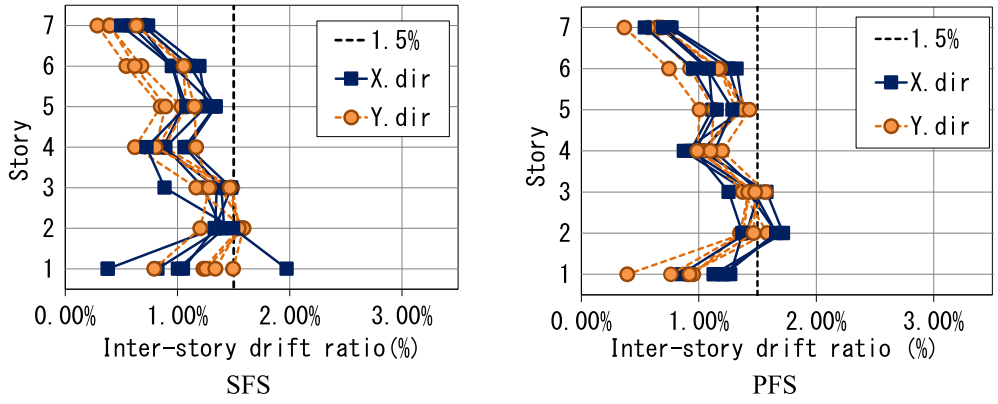

Fig. 7. Mean values of maximum inter-story drift ratios under three seismic ground motions.

buildings with the similar sizes as examined here is 131 kg/m^2. Although the ratio of equivalent steel volume of BRBs to the total volume in the building is relatively high as approximately 40% in both 1st SDSs, the total steel weights in SDSs are approximately 10% lower than the statistic average. This shows the efficiency and usefulness of the proposed MSLS algorism for structural design of steel buildings associated with BRBs considering the section sizes in the main frames and the BRB strength and locations simultaneously as the design variables.

5.6. Lateral stiffness

Focusing on the 1st SDSs of SFS and PFS, the first natural periods T_1 are 0.89 and 0.94 sec in SFS, and 0.93 and 0.91 sec in PFS. On the other hand, for the main frames without BRBs, the first natural periods T_{MF1} are 2.69 and 3.21 sec in SFS, and 4.72 and 3.53 sec in PFS. Without BRBs, the lateral stiffness of PFS is lower than that of SFS. Assuming that the reciprocal of square of first natural period is proportional to the lateral stiffness, the ratio of elastic lateral stiffness with BRBs K_a to the stiffness K_f of main frame is calculated for each frame. The values of K_a/K_f are 8.2 and 10.7 in SFS, and 24.4 and 14.1 in PFS. Also, the ratio of lateral force carried by BRBs is more than 65% for SFS and more than 85% for PFS. These values are significantly larger, especially in PFS, than those studied in the previous research [1,14].

The values of T_1, T_{MF1} and K_a/K_f for 1st to 5th SDSs are shown in

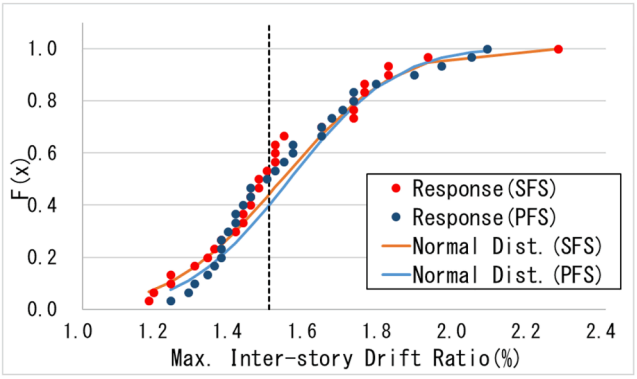

Fig. 8. Cumulative distribution of inter-story drift ratio.

Table 4 and 5. Looking at the values of K_a/K_f, they are greater than those of PFS. Therefore, lateral stiffness of the main frames is relatively lower in SDSs of PFS. This fact results in the larger residual inter-story drift ratios and ductility factors in PFS. The large value of K_a/K_f, i.e., the large lateral stiffness of BRBs, in SDSs is also observed from the small section sizes in the main fame in Table 4 and 5, e.g., small beam heights between 300 and 450 mm. Possible reasons for this are the relatively small and uniform column spacing (6.4 m), and wide range of possible BRB locations. On the other hand, the ductility factors of SDSs at the limit state in CRLS and RHA are not excessive. Also, the residual displacements simulated in RHA are within the tolerance. Additionally taking into account the efficiency in equivalent steel volume V_{eq} of SDSs evaluated in the previous section, rationale of structural design of steel buildings with BRBs under higher K_a/K_f is implied.

5.7. SDSs with higher demand levels

The SDSs under greater demand spectra are derived in the same procedure as described in the previous sections. S_a and S_d in the demand spectrum in Fig. 5 is scaled by the factor 1.25 and 1.5, respectively. Hereinafter, the SDSs corresponding to the original and greater demands are denoted as 1.0-, 1.25- and 1.5-SDS, respectively. Also, EF-SDSs are obtained under original spectrum shown in Fig. 5 with additional design constraint that the beams and columns, i.e., the main frame members, remain elastic at the limit-state. It is confirmed that these SDSs satisfy the ASD and CRLS constraints. The capacity at the safety limit in all SDSs is nearly equal to the demand as shown in Fig. 6 for the 1.0-SDSs.

The values of equivalent steel volume for each type of members of the 1st 1.25-, 1.5-, EF-SDSs are shown in Fig. 11. The increase of the total equivalent steel volume V_{eq} with respect to the increase of demand spectrum is almost the same in SFS and PFS, and V_{eq} is nearly proportional to the demand level. It implies that the design of structural members excluding the secondary beams is primarily controlled by the seismic design. V_{eq} of EF-SDSs is between those of 1.0-SDSs and 1.25-SDSs both in SFS and PFS, and is 119% (SFS) and 109% (PFS) of that of 1.0-SDSs. Therefore, the elastic main frame constraint does not drastically increase the steel volume. The maximum ductility factors in members of 1.0- and EF-SDSs at the limit-state in CRLS are also shown in Table 6. Those values of main frames are almost less than 1.0. Therefore,

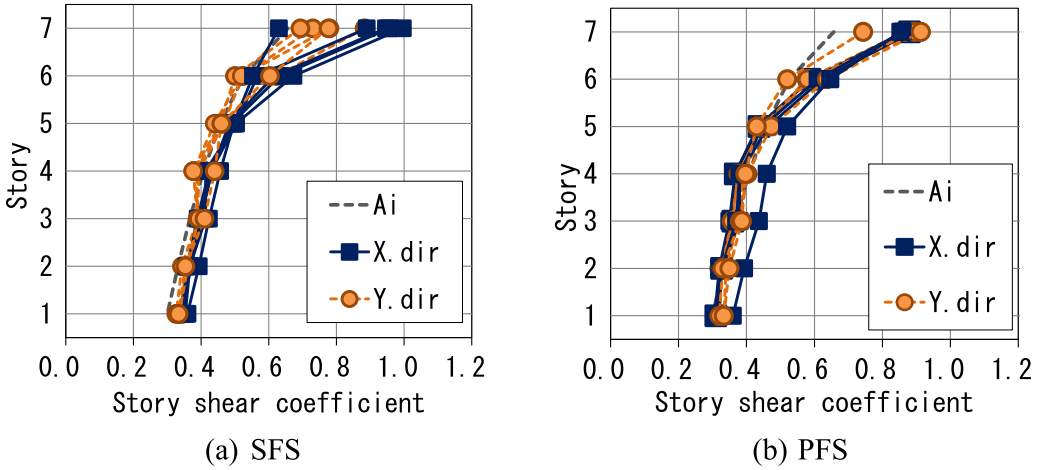

Fig. 9. Mean values of maximum story shear coefficients under three seismic ground motions.

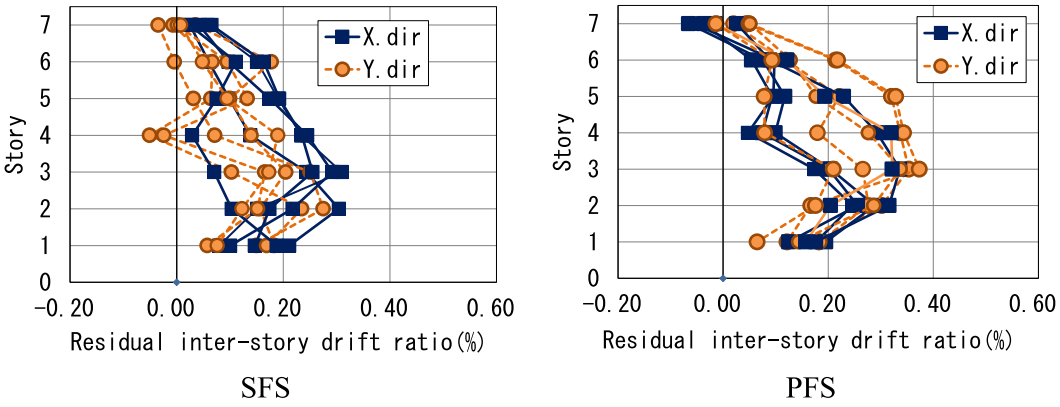

Fig. 10. Mean values of maximum residual inter-story drift ratios under three seismic ground motions.

Table 6
Ductility factors in response history analyses.

	SDS	1st		2nd		3rd		4th		5th		EF-SDS	
	Direction	X	Y	X	Y	X	Y	X	Y	X	Y	X	Y
SFS	Column	–	–	–	–	–	1.14	–	–	2.53	–	–	–
	Beam	1.40	2.09	1.55	1.33	1.65	1.42	2.13	1.92	3.59	1.47	1.10	1.07
	BRB	6.84	7.74	7.27	7.19	6.83	7.96	6.75	7.19	7.28	5.85	7.05	7.05
PFS	Column	–	1.03	1.14	–	–	–	1.25	–	2.12	–	–	1.08
	Beam	2.58	1.81	2.17	2.06	2.09	2.36	2.40	2.17	3.02	2.54	1.62	1.51
	BRB	8.64	7.05	8.08	7.84	7.54	8.21	8.29	7.09	6.84	6.72	6.64	6.90

"– " indicates the ductility ratios less than one. (i.e., no yielding in the members).

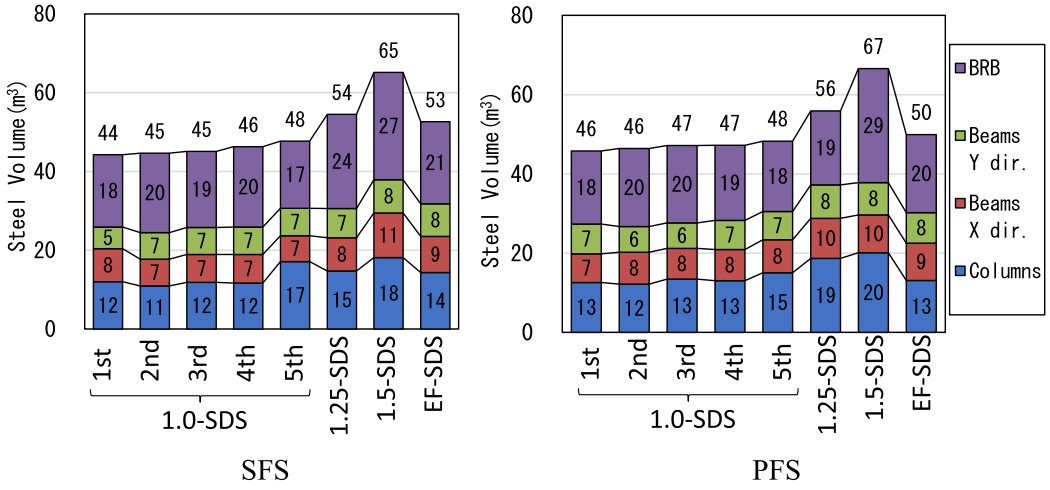

Fig. 11. Steel volume of SDSs.

structural design providing the role of energy dissipation to BRBs separately, while the main frame remains intact under large earthquakes, is achieved in CRLS of EF-SDSs. The RHA under the three ground motions shown in Fig. 5 are conducted to these SDSs. The average values of maximum ductility factors in members for the three ground motions are 2.09 and 2.58 for SFS and PFS in 1.0-SDSs, and 1.10 and 1.51 for SFS and PFS in EF-SDSs. These values are smaller in EF-SDSs; however, the mean values of maximum residual inter-story drift ratios for the three ground motions are 0.30% and 0.29% for SFS and PFS in 1.0-SDSs, and 0.25% and 0.47% for SFS and PFS in EF-SDSs. The residual inter-story drift ratios of 1.0-SDSs are smaller than those of EF-SDSs in SFS, but it is opposite in PFS. Therefore, the smaller ductility factors in the main frames do not necessarily correspond to smaller residual inter-story drift ratios.

Comparing 1.0-, 1.25- and 1.5-SDSs, the first natural period becomes smaller as the seismic demand is increased. The values of K_a/K_f of SDSs vary between 5 and 17, and no obvious relationships are observed between the stiffness ratios and seismic demands. The average values of maximum inter-story drift ratios under the three ground motions in Fig. 5, which are 0.78% and 0.85% for SFS and PFS, respectively, in 1.5-SDSs are shown in Fig. 12. It is seen that the inter-story drift ratio decreases due to the increase of the seismic demand. Thus, the SDSs with higher seismic performance are successfully derived.

6. Conclusions

A structural design algorithm is proposed to find SDSs using the MSLS method for steel buildings associated with BRBs. The strengths and locations of BRBs in addition to the section sizes of structural members are considered as discrete design variables. The steel volume including BRBs is minimized as an objective function. The SDSs satisfy serviceability constraints under the ASD process against sustained and

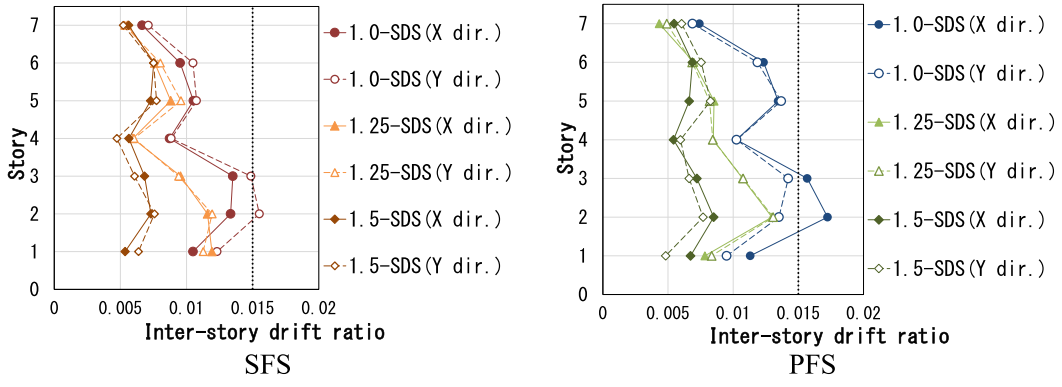

Fig. 12. Maximum inter-story drift ratios in 1st 1.0–1.25- and 1.5-SDSs.

design seismic loads, as well as limit-state constraints under the CRLS for large earthquakes. The SDSs of a seven-story office building in the SFS and PFS are derived, where the columns are square hollow structural sections and most of the beam-to-column connections are moment connections in SFS, and the columns are I-shaped sections and the moment connections are limitedly used in the perimeter frames in PFS.

Applying the proposed design procedure, the entire seismic resisting systems of the buildings composed of the main frames and BRBs are designed taking into consideration the seismic energy dissipation effect of BRBs using CRLS. It is confirmed that the SDSs are successfully designed satisfying almost all of the practical structural design constraints. The proposed algorithm can be a good tool to find the structural characteristics of rational steel building design with respect to various design conditions.

The equivalent steel volume of the 1st SDS of PFS is 4% larger than that of the SFS. SFS is slightly advantageous in terms of the equivalent steel volume in the examined building; however further studies in various aspects such as fabrication cost or irregularity in the plans and shapes are needed for more general comparative structural characteristic evaluation between SFS and PFS. The ratio of equivalent steel volume of BRBs to the total volume in the building is relatively high as approximately 40% in SDSs of both SFS and PSF; however, the total steel weight in SDSs is approximately 10% smaller than the statistic average of existing buildings.

The ratios of seismic lateral forces carried by BRBs in the elastic state are more than 65% of the total frame. The ratios of elastic lateral stiffness provided by BRBs with respect to the stiffness of main frames (K_a/K_f) are 8.2 and 10.7 for X and Y dir., respectively, in SFS and 24.4 and 14.1 in PFS, which are larger than the standard design. Rationale of structural design of steel buildings with BRBs under higher K_a/K_f is implied.

Seven different combinations of BRB locations are observed in total in the top five SDSs of SFS and PFS. The difference of equivalent steel volume between the 1st and 5th SDSs is relatively small as 7.8% in SFS and 5.4% in PFS. Therefore, the BRB locations do not necessarily govern the overall steel volume.

The increase of equivalent steel volume with respect to the increased demand spectra is nearly proportional to the demand level both in SFS and PFS, because the design of structural members is primarily controlled by the seismic design. The elastic main frame constraint does not drastically increase the steel volume, and it is less than that of 1.25-SDSs. The ductility factors in the main frames in EF-SDS are smaller than those in 1.0-SDSs; however it does not correspond to smaller residual inter-story drift ratios.

Declaration of Competing Interest

The authors declare that they have no known competing financial interests or personal relationships that could have appeared to influence the work reported in this paper.

Acknowledgements

The authors gratefully acknowledge Dr. Tomohiro Mikami, Obayashi Corporation for the discussion regarding practical steel building design using the buckling restrained braces, and Ms. Yuka Yabuki, Ms. Yumi Goto, Ms. Akari Hayashi and Mr. Kazuki Saito, graduate and undergraduate students at Tokyo Metropolitan University for the assistance in the numerical simulations. The research is financially supported by JSPS KAKENHI Grant Number JP21K04337.

References

[1] Japan Society of Seismic Isolation. Design and Construction Manual for Passive Control System 3rd Edition. 2013. (in Japanese).
[2] Takeuchi T, Wada A. Buckling-Restrained Braces and Applications. Japan Society of Seismic Isolation 2017.
[3] Kiggins S, Uang C-M. Reducing residual drift of buckling-restrained braced frames as a dual system. Eng Struct 2006;28(11):1525–32. https://doi.org/10.1016/j.engstruct.2005.10.023.
[4] Sabelli R, Mahin S, Chang C. Seismic demands on steel braced frame buildings with buckling-restrained braces. Eng Struct 2003;25(5):655–66. https://doi.org/10.1016/S0141-0296(02)00175-X.
[5] Barbagallo F, Bosco M, Marino EM, Rossi pp. Seismic design and performance of dual structures with BRBs and semi-rigid connections. J Constr Steel Res 2019;158:306–16. https://doi.org/10.1016/j.jcsr.2019.03.030.
[6] Freddi Fabio, Ghosh Jayadipta, Kotoky Needhi, Raghunandan Meera. Device uncertainty propagation in low-ductility RC frames retrofitted with BRBs for seismic risk mitigation. Earthquake Eng Struct Dyn 2021;50(9):2488–509. https://doi.org/10.1002/eqe.v50.910.1002/eqe.3456.
[7] Freddi F, Tubaldi E, Ragni L, dall'Asta A. Probablistic performance assessment of low-ductility reinforced concrete frames retrofitted with dissipative braces. Earthquake Eng Struct Dyn 2013;42(7):993–1011. https://doi.org/10.1002/eqe.2255.
[8] Mazzolani FM, Corte GD, D'Aniello M. Experimental analysis of steel dissipative bracing systems for seismic upgrading. J Civ Eng Manag 2009;15(1):7–19. https://doi.org/10.3846/1392-3730.2009.15.7-19.
[9] Freddi F, Tubaldi E, Zona A, Dall'Asta A. Seismic performance of dual systems coupling moment-resisting and buckling-restrained braced frames. Earthquake Eng Struct Dyn 2021;50(2):329–53. https://doi.org/10.1002/eqe.3332.
[10] Mehdipanah A, Mirghaderi R, Tabatabaei SAR. Seismic performance of stiffness-based designed buckling-restrained braced frame and special moment-resisting frame dual systems. Struct Infrastruct Eng 2016;12(8):918–35. https://doi.org/10.1080/15732479.2015.1071854.
[11] Sarno LD, Elnashai AS. Bracing systems for seismic retrofitting of steel frames. J Constr Steel Res 2009;65(2):452–65. https://doi.org/10.1016/j.jcsr.2008.02.013.
[12] Terazawa Yuki, Takeuchi Toru. Optimal damper design strategy for braced structures based on generalized response spectrum analysis. J Struct Constr Eng (Trans AIJ) 2019;2(4):477–93. https://doi.org/10.1002/jar3.v2.410.1002/2475-8876.12122.
[13] Park K, Oh BK, Park HS. GA-based multi-objective optimization for retrofit design on a multi-core PC cluster. Comput-Aided Civ Infrastruct Eng 2015;30(12):965–80. https://doi.org/10.1111/mice.12176.
[14] Inoue K, Kuwahara S. Optimum strength ratio of hysteretic damper. Earthquake Eng Struct Dyn 1998;27(6):577–88. https://doi.org/10.1002/(SICI)1096-9845(199806)27:6%3C577::AID-EQE743%3E3.0.CO;2-U.
[15] Balling Richard J, Balling Lukas J, Richards Paul W. Design of buckling-restrained braced frames using nonlinear time history analysis and optimization. J Struct Eng 2009;135(5):461–8. https://doi.org/10.1061/(ASCE)ST.1943-541X.0000007.
[16] Rezazadeh F, Talatahari S. Seismic energy-based design of BRB frames using multi-objective vibrating particles system optimization. Structures 2020;24(8):227–39. https://doi.org/10.1016/j.istruc.2020.01.006.
[17] Abedini H, Vaez SRH, Zarrineghbal A. Optimum design of buckling-restrained braced frames. Structures 2020;25:99–112. https://doi.org/10.1016/j.istruc.2020.03.004.
[18] Takagi J, Ohsaki M. Comparison of structural characteristics of office buildings composed of space and perimeter frame systems. J Struct Constr Eng (Trans AIJ) 2015;80(715):1469–78. https://doi.org/10.3130/aijs.80.1469 (in Japanese).
[19] Takagi Jiro, Obana Ruka, Ohsaki Makoto. Superior design solutions of section sizes in steel buildings for different lateral frame systems and column shapes. Japan Architect Rev 2020;3(4):445–58. https://doi.org/10.1002/jar3.v3.410.1002/2475-8876.12156.
[20] TAKAGI Jiro, CAO Yongsheng, YABUKI Yuka, OHSAKI Makoto. Superior design solutions of steel buildings including strength and location of buckling restrained braces in design variables座屈拘束ブレースの耐力と配置を設計変数に含めた鋼構造建物の優良設計解. J Struct Constr Eng (Trans AIJ) 2021;86(782):642–50. https://doi.org/10.3130/aijs.86.642.
[21] Mele E, Sarno LD, Luca AD. Seismic behavior of perimeter and spatial steel frames. J Earthquake Eng 2004;8(3):457–96. https://doi.org/10.1080/13632460409350497.
[22] Mason BF, Kasai K, Ooki Y. Relative performance of Kobe and Northridge WSMF buildings. Earthquake Spectra 2006;22(4):1081–1101. https://doi.org/10.1193%2F1.2359743.
[23] Tagawa Hiroyuki, MacRae Gregory, Lowes Laura. Probabilistic evaluation of seismic performance of 3-story 3D one- and two-way steel moment-frame structures. Earthquake Eng Struct Dyn 2008;37(5):681–96. https://doi.org/10.1002/(ISSN)1096-984510.1002/eqe.v37:510.1002/eqe.778.
[24] Poole DJ, Allen CB, Rendall TCS. A genericframework for handling constraints with agent-based optimization algorithms and application to aerodynamic design. Optim Eng 2017;18(3):659–91. https://link.springer.com/article/10.1007/s11081-016-9343-0.
[25] Pedamallu CS, Ozdamar L. Investigating a hybrid simulated annealing and local search algorithm for constrained optimization. Eur J Oper Res 2008;185(3):1230–45. https://doi.org/10.1016/j.ejor.2006.06.050.
[26] Lange Volker A, Fender Johannes, Duddeck Fabian. Relaxing high-dimensional constraints in the direct solution space method for early phase development. Optim Eng 2018;19(4):887–915.
[27] Bruneau M, Uang CM, Sabelli R. Second Edition Ductile Design of Steel Structures. Mc-Graw Hill Education 2011.
[28] Architectural Institute of Japan. AIJ Design Standard for Steel Structures–Based on Allowable Stress Concept– (2005 Edition). 2017.10.

[29] American Society of Civil Engineers (ASCE). Minimum Design Loads and Associated Criteria for Buildings and Other Structures (ASCE/SEI 7-16). 2016.
[30] National Institute for Land and Infrastructure Management (NILIM), et al. Explanation Book of Structural Technology Standard of Buildings. 2015.6. (in Japanese).
[31] Freeman SA. Prediction of Response of Concrete Buildings to Severe Earthquake Motion. Douglas McHenry International Symposium on Concrete and Concrete Structures, SP-55, American Concrete Institute, Detroit, Michigan. pp. 589–605, 1978.
[32] Kuramoto H. et al., Predicting the Earthquake Response of Building Using Equivalent Single Degree of Freedom System. Proceeding of 12th World Conference on Earthquake Engineering, Auckland, New Zealand, 2000, Paper No. 1039 (CD-ROM).
[33] Building Guidance Division, Housing Bureau, the Ministry of Land, Infrastructure and Transport (MLIT) et al. Calculation Examples and Explanation for Calculation of Response and Limit Strength 2001, Kougaku-Tosho, 2006.6 (in Japanese).
[34] Kubo M, Pedroso JP. Metaheuristics, a programming guide. Kyoritsu Shuppan Co., Ltd., Japan, 2009 (in Japanese).
[35] Nippon Steel. Handbook Library. accessed 2021. https://www.nipponsteel.com/product/construction/handbook/ (in Japanese).
[36] Midas iGEN Ver. 900R1x, MIDAS Information Technology. 2021.
[37] JFE Civil Engineering & Construction Corp., Tube-in-Tube Buckling-Restrained Braces. 2016. (in Japanese).
[38] The Building Center of Japan. Tube-in-Tube Buckling-Restrained ST0010-05. 2016.8. (in Japanese).
[39] SNAP Ver.7.0.1.6, Kozo System, Inc.. 2019.
[40] Hashimoto S, Maruki K. Study on Material Quantities for Building Structures and Their Variations: Part 2 Steel Office Buildings, Summaries of Technical Papers of Annual Meeting, Architectural Institute of Japan. F-1, Urban Planning and Design, Building Economy / Housing Problems. pp. 1217–1218, 2008.7 (in Japanese).